9-9-2024

High-Frequency-Based Transmission Line Percentage Differential Protection with Traveling Wave Alignment

Igor F. Prado
Universidade Estadual de Santa Cruz

Flavio Costa
Michigan Technological University, fbcosta@mtu.edu

Kleber M. Silva
Universidade de Brasília

Rodrigo P. Medeiros
Universidade Federal do Rio Grande do Norte

Bruce A. Mork
Michigan Technological University, bamork@mtu.edu

IEEE Access
Multidisciplinary | Rapid Review | Open Access Journal

Received 9 August 2024, accepted 25 August 2024, date of publication 9 September 2024, date of current version 20 September 2024.

Digital Object Identifier 10.1109/ACCESS.2024.3456040

RESEARCH ARTICLE

High-Frequency-Based Transmission Line Percentage Differential Protection With Traveling Wave Alignment

IGOR F. PRADO[1,2], (Member, IEEE), FLAVIO B. COSTA[3], (Member, IEEE), KLEBER M. SILVA[4], (Senior Member, IEEE), RODRIGO P. MEDEIROS[2], (Member, IEEE), AND BRUCE A. MORK[3], (Senior Member, IEEE)

[1]Department of Engineering and Computer, State University of Santa Cruz, Ilhéus, Bahia 45662-900, Brazil
[2]Department of Electrical Engineering, Federal University of Rio Grande do Norte, Natal 59078-970, Brazil
[3]Department of Electrical and Computer Engineering, Michigan Technological University (MTU), Houghton, MI 49931, USA
[4]Department of Electrical Engineering, University of Brasília, Brasília 70910-900, Brazil

Corresponding author: Igor F. Prado (ifprado@uesc.br)

ABSTRACT This paper presents a wavelet-based differential protection algorithm for transmission lines. It uses restraint and operating components obtained with high-frequency components of a few kHz from instantaneous energy values of the real-time boundary stationary wavelet transform instead of low-frequency components from phasor estimation. It does not require capacitive current suppression as well. Therefore, the proposed method overcomes the limitations of conventional percentage differential protection. Furthermore, the proposed technique uses traveling wave theory to perform the current sample alignment at a few kHz, thereby, not requiring the global positioning system (GPS). The performance of the proposed method is evaluated through extensive simulation of 21,450 realistic cases contemplating internal faults, external faults, high-impedance faults, faults with outfeed, line energization, and CT saturation. When compared to a conventional percentage differential protection the proposed protection method is able to detect faults up to 5 times faster, presenting a success rate of 100% against 98,2% achieved by the conventional one.

INDEX TERMS Percentage differential protection, transmission line, traveling wave, wavelet transform.

I. INTRODUCTION

Transmission lines are the main connecting element between generation systems and energy consumption centers, responsible for transporting large amounts of power. Due to its large extension, it is the element most susceptible to failures, usually associated with natural factors [1]. Therefore, protection systems have converged towards increasingly faster and more selective actions to maintain supply continuity and preserve system stability, mitigating damage to equipment [2]. In this context, differential protection has been applied to provide unitary protection with no intentional time delay.

Due to the electrical characteristics of transmission lines related to loading and capacitive currents, conventional differential protection methods can compromise safety and sensitivity in fault detection. References [3], [4] and [5] incorporate algorithms based on current and voltage measurements at the terminals that compensate for charging and capacitive current effects, making conventional protections more robust at the cost of increasing the complexity of the protection algorithm. In general, the traditional percentage differential protection has limitations in detecting high-impedance faults and outfeed fault conditions. Therefore, research has been developed to increase sensitivity by adapting the operating and restriction regions according to the system operation, and fault conditions [6], [7], [8].

Sample alignment between current terminals is essential for differential protection operation. Usually, the synchronizing source can be Global Navigation Satellite Systems (GNSS), or Precision Time Protocol (PTP) via IEEE

The associate editor coordinating the review of this manuscript and approving it for publication was Arturo Conde.

Std. 1588 [9]. However, its accuracy may vary over time due to changes in temperature, electrical and magnetic interference, oscillator age, and altitude [10].

In order to make the differential protection more robust against the loss of the GPS signal, [11] developed a GPS signal failure detection algorithm based on symmetrical components that improve the stability of the line differential protection. The traditional alpha-plane differential protection [12], [13], [14], also has robustness for delays and misalignments between samples, which is based on a ratio between phasor currents measured at the line terminals, achieving greater sensitivity for CT saturation and faults with outfeed conditions. However, traditional line differential protection methods are based on phasor estimation, which generates an intrinsic delay due to the window sizes used to calculate the phasors, something around one cycle [15].

Over the last few decades, research has focused on time domain differential protection that does not require phasor estimation [16]. In [17] and [18], the discrete wavelet transform (DWT) is used to protect and locate faults in the transmission system. Nevertheless, the sensitivity of conventional wavelet transforms is affected by noise and for detecting faults with high impedance or faults with reduced transients for specific fault inception angles as described in [19] and [20]. In [21], differential protection based on instantaneous values is implemented using window data of at least a quarter of a cycle.

New transmission line protection schemes, such as the two-terminal traveling wave-based protection schemes proposed in [20], [22], and [23], have been implemented in commercially available relays, speeding up the protection operating time. Moreover, they cannot effectively protect the entire line, such as faults close to the line terminals [23], faults with specific fault inception angles [19], faults with high fault resistance, and cross-country faults.

Recently, the real-time stationary wavelet transform with border effects (RT-BSWT) has been used as a tool for implementing differential protections based on high-frequency components, presenting good performance on busbar and power transformer protections [24], [25]. The RT-BSWT overcomes limitations of the classical wavelet transform, presenting no time delay in fault detection [19] and robustness to high-impedance faults [26]. However, it has not been used for transmission line differential protection to the best of the author's knowledge.

This paper proposes a transmission line differential protection based on high-frequency components extracted by means of the RT-BSWT instead of low-frequency components extracted by traditional phasor filtering techniques. The main purpose is to take advantage of the transmission line differential protection principle and recreate the traditional current differential element (87L) by using the differential wavelet coefficient energies with border effects. Consequently, besides fast protection, its performance is not affected by the main issues of conventional strategies, such as the line capacitive current and CT saturation. Indeed, the protection algorithm uses only concepts of differential protection with signals sampled at a few kHz instead of MHz, which is usually required by traveling wave-based protections. In addition, it has a well-defined characteristic for trip decision, not based only on a wavefront, being more robust, therefore, to misalignments, small communication failures, faults close to the line terminals, faults with high resistance, and faults with specific fault inception angles

This paper also presents innovations in wavelet-based signal processing, proposing an enhanced energy component that is more sensitive than previous works [16-19]. The protection method performance is validated through realistic simulations in a 230 kV transmission system for external and internal faults with variations of fault resistance and fault inception angle, considering the presence and the absence of CT saturation and energization condition. The implemented protection system consists of two protective relays interconnected by a realistic asymmetric communication system, which considers the communication channel latency with deterministic and probabilistic time delays. As a result, the proposed method presented protection with a success rate of 100% and an average operating time lower than the conventional percentage differential protection.

II. PROPOSED LINE DIFFERENTIAL PROTECTION

Fig. 1 depicts the flowchart of the proposed wavelet-based transmission line differential protection scheme, named here

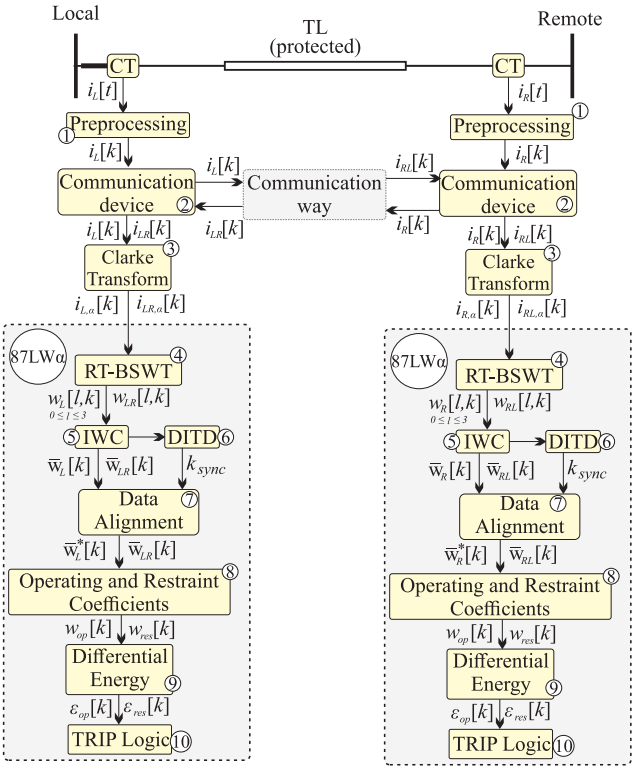

FIGURE 1. Flowchart of the proposed wavelet-based line differential protection 87LW.

as 87LW protection unit. A communication system performs the connection between local and remote relays. These relays operate in parallel and independently, such that each relay has full autonomy for issuing the TRIP. All proposed 87LW protection unit steps are explained in the remainder of this section, taking the local terminal as a reference.

A. BASIC PRE-PROCESSING (BLOCK 1)

The basic pre-processing block converts instantaneous local currents $i_L[t] = \{i_{AL}[t], i_{BL}[t], i_{CL}[t]\}$ measured in local CTs to the respective time-discrete local current samples $i_L[k] = \{i_{AL}[k], i_{BL}[k], i_{CL}[k]\}$ by means of anti-aliasing filters and AD converters. Likewise, the time-discrete remote current samples are given by $i_R[k] = \{i_{AR}[k], i_{BR}[k], i_{CR}[k]\}$.

B. COMMUNICATION SYSTEM (BLOCK 2)

Fig. 2 depicts the lattice diagram of an internal fault located d km from the local bus on a transmission line with length l. The fault takes place at t_F. Thereafter, traveling waves propagate from the fault point toward the local and remote line terminals with limited propagating velocity. Therefore, the fault effects, such as fault-induced transients, will be detected from the fault inception discrete-times $t_{FL} = k_{FL}/f_s$ and $t_{FR} = k_{FR}/f_s$ in the local and remote relays, respectively.

The communication system sends all current samples from the remote terminal $i_R[k] = \{i_{AR}[k], i_{BR}[k], i_{CR}[k]\}$ to the local one. At the local terminal, these currents are $i_{LR}[k] = \{i_{ALR}[k], i_{BLR}[k], i_{CLR}[k]\}$, which are remote-sent currents. Besides remote-sent currents i_{LR} present the same information of i_R in an ideal communication system, the time stamp has a communication system delay, which includes the inherent delay of communication devices and propagation time in communication channels. As a consequence, the remote fault inception time seen from the local line terminal, namely t_{FLR}, is different from t_{FR} (Fig. 2).

The emulated communication system considers two-stage delays: 1) a deterministic delay associated with the propagation of the signals in a fiber optic cable with length equal to the transmission line length ($t_{RL} = t_{LR} = l/(0.6814c)$), where c is the light speed in m/s [23]; 2) a fixed delay of 3 ms required by the communication equipment for coding and signal processing at both line terminals (sender and receiver) added to a non-deterministic delay of up to 1 ms (RDN) to make the model realistic [23]. Thus, the time delay of the signal sent by the communication system, in seconds, is computed as follows:

$$D_c = 0.003 + 0.001 * RDN + l/(0.6814c)[s] \quad (1)$$

The average time spent on the communication system is equivalent to 4.5 ms with a standard deviation of 0.5 ms. Communication delay in long-distance transmission lines is a crucial parameter for ensuring the efficient and reliable operation of the electrical system, as the greater the distance between terminals, the longer the detection of a fault in the transmission line will take. The communication delay is

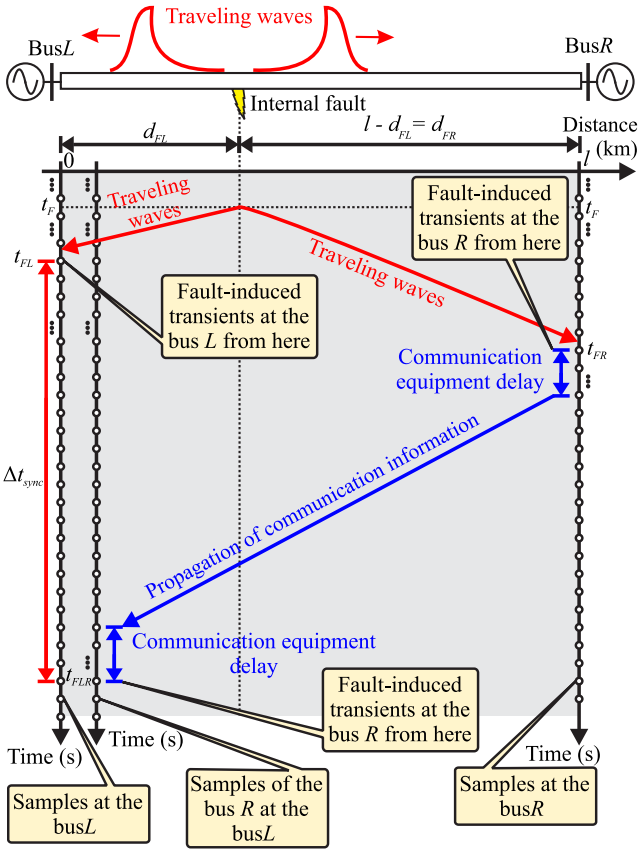

FIGURE 2. Lattice diagram for a fault in the protected TL and the effect of latency on communication between line terminals.

inherent to transmission line differential protection methods, and it is identical for both the proposed method and the existing methods. In general, the implementation of high-speed optical communication technologies is a way to overcome communication overheads and delays associated to fault detection in long-distance transmission lines.

C. CLARKE TRANSFORM (BLOCK 3)

The Clarke transform provides the alpha components of the local currents $i_{L,\alpha}[k] = \{i_{AL,\alpha}[k], i_{BL,\alpha}[k], i_{CL,\alpha}[k]\}$ as follows [27]:

$$\begin{bmatrix} i_{AL,\alpha}[k] \\ i_{BL,\alpha}[k] \\ i_{CL,\alpha}[k] \end{bmatrix} = \sqrt{\frac{2}{3}} \begin{bmatrix} 1 & -\frac{1}{2} & -\frac{1}{2} \\ -\frac{1}{2} & 1 & -\frac{1}{2} \\ -\frac{1}{2} & -\frac{1}{2} & 1 \end{bmatrix} \begin{bmatrix} i_{AL}[k] \\ i_{BL}[k] \\ i_{CL}[k] \end{bmatrix}. \quad (2)$$

The alpha-mode remote-sent currents $i_{LR,\alpha}[k] = \{i_{ALR,\alpha}[k], i_{BLR,\alpha}[k], i_{CLR,\alpha}[k]\}$ are computed similarly by using $i_{LR}[k]$ instead of $i_L[k]$.

D. RT-BSWT (BLOCK 4)

The inner product between the last L samples of a current i and the wavelet filter h_ψ with L coefficients results in the

RT-BSWT wavelet coefficients as follows [19], [28]:

$$w[l,k] = \frac{1}{\sqrt{2}} \sum_{n=0}^{L-1} h_\psi[n] \mathring{i}[k-L+n+1+l], \qquad (3)$$

where $0 \leq l < L; k > \Delta k - 1$; $\mathring{i}$ is a periodic signal of i in Δk samples, i.e., $\mathring{i}[k+m] = i[k-\Delta k+m]$ with $m \in \mathbb{Z}$; $w[0,k] = w[0]$ is the kth wavelet coefficient of the conventional SWT; $w[l \neq 0, k] = w[l]$ are the $L-1$ additional boundary wavelet coefficients.

The RT-BSWT wavelet coefficients of local and remote-sent currents $\{w_{AL}, w_{BL}, w_{CL}, w_{ALR}, w_{BLR}, w_{CLR}\}$ are computed with the respective alpha-mode local and remote-sent currents $\{i_{AL,\alpha}, i_{BL,\alpha}, i_{CL,\alpha}, i_{ALR,\alpha}, i_{BLR,\alpha}, i_{CLR,\alpha}\}$ by using (3).

E. IMPROVED WAVELET COEFFICIENTS (BLOCK 5)

For each sampling k, the RT-BSWT decomposition results in L wavelet coefficients in the first wavelet decomposition level, instead of just one wavelet coefficient obtained by using the SWT [19], [20], [28]. Furthermore, at least one of the L RT-BSWT wavelet coefficients of the local and remote-sent currents are sensitive to fault-induced transients. Thus, selecting the most expressive wavelet coefficient can be an issue. However, this paper proposes the combination of all L RT-BSWT wavelet coefficients in a single coefficient to maximize the wavelet-based relay performance regarding fault detection and simplify the protection algorithm.

Considering the Daubechies mother wavelet with four coefficients (db4), which has been reported as one of the wavelet filters most sensitive to fault-induced transients [19], [20], [28], this paper proposes the improved wavelet coefficient as follows:

$$\overline{w}[k] = w[0,k] + w[1,k] - w[2,k] - w[3,k], \qquad (4)$$

making it sensitive to fault-induced transients in signals with a high degree of noise and in fault situations with overdamped transients.

Based on (4), the block 5 in Fig. 1 process, per sampling k, the wavelet coefficients $w = \{w_{AL}, w_{BL}, w_{CL}, w_{ALR}, w_{BLR}, w_{CLR}\}$ and provides the improved wavelet coefficients $\overline{w}=\{\overline{w}_{AL}, \overline{w}_{BL}, \overline{w}_{CL}, \overline{w}_{ALR}, \overline{w}_{BLR}, \overline{w}_{CLR}\}$ per sampling interval. For instance, Fig. 3 depicts the local currents and the respective wavelet coefficients w and $\overline{w}$ for a single-line-to-ground (SLG) fault in phase A (AG fault) with a fault inception angle of 0° and with fault resistance equal to 500 Ω. This fault presents damped fault-induced transients, which challenge fault detection methods. Indeed, the conventional wavelet coefficient $w_{AL}[0]$ in Fig. 3(b) does not react to this fault, being sensible only to noise. Conversely, the RT-BSWT wavelet coefficients $\{w_{AL}[1], w_{AL}[2], w_{AL}[3]\}$ in Fig 3(b) reacted to the fault. Nevertheless, the improved wavelet coefficient $\overline{w}_{AL}$ in Fig 3(b) was the most sensitive among them, identifying fault inception time accurately even in this critical fault situation. The fault inception time is required by the proposed method to align local and remote currents, and its detection must be as accurate as possible.

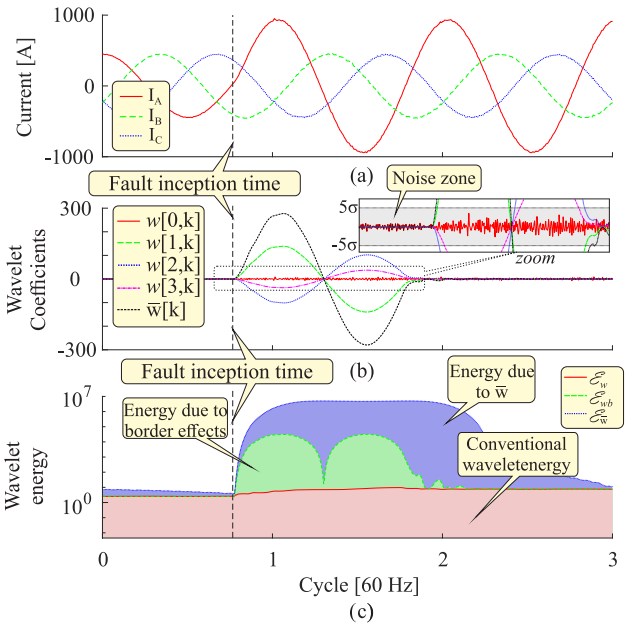

FIGURE 3. Wavelet signals during a fault: (a) local phase currents; (b) wavelet coefficients $w_{AL}[0,k]$, $w_{AL}[1,k]$, $w_{AL}[2,k]$, $w_{AL}[3,k]$, and $\overline{w}_{AL}[k]$; (c) wavelet Energies.

F. DISTURBANCE DETECTION (BLOCK 6)

During the steady-state, the RT-BSWT wavelet coefficients usually present a Gaussian distribution with a mean of approximately zero ($\mu_w \approx 0$) and a specific standard deviation (σ_w), denoted as $N(0, \sigma_w^2)$ [20]. Therefore, based on the central limit theorem [29], the improved wavelet coefficients $\overline{w}$ also present a Gaussian distribution during the steady-state with mean equal to zero and standard deviation $\sigma_{\overline{w}}$. Therefore, the following thresholds can be used to detect transients and reject noise:

$$-5\sigma_{\overline{w}} > \overline{w}[k] > 5\sigma_{\overline{w}}, \qquad (5)$$

In other words, when (5) is fulfilled, a fault or any other non-stationary disturbance is detected.

G. FAULT INCEPTION TIME ALIGNMENT (BLOCK 7)

Conventional transmission line differential protection functions and other types of protections, such as traveling wave-based methods, require synchronization of the signals measured in all line terminals with GPS [30], [2]. However, solutions for artificial synchronization without GPS have been proposed, such as synchronization based on the first wavefront arrival time of traveling waves at transmission line terminals [31]. Considering the fault-induced transients can be properly extracted using signals sampled at a few kHz, this paper proposes the alignment between the local and remote current samples based on the fault inception time detection in each current, disregarding the need for a GPS.

When a disturbance takes place, transients are launched from the fault point toward line terminals. By using (5), these transients are detected in times t_{FL} and t_{FLR} and then the current sample alignment is performed.

Considering the lattice diagram in Fig. 2, the local and remote-sent transient inception discrete-times t_{FL}=k_{FL}/f_s and t_{FLR}=k_{FLR}/f_s, termed as reference local and remote-sent times respectively, are defined when a transient disturbance is detected at the local terminal with the improved wavelet coefficients $\overline{w}_L$=$\{\overline{w}_{AL}, \overline{w}_{BL}, \overline{w}_{CL}\}$ and at the remote-sent current signals with the improved wavelet coefficients $\overline{w}_{LR}$=$\{\overline{w}_{ALR}, \overline{w}_{BLR}, \overline{w}_{CLR}\}$ by using (5), as follows:

$$|\overline{w}_L[k]| > 5\sigma_{\overline{w}} \Rightarrow k_{FL} = k, \tag{6}$$
$$|\overline{w}_{LR}[k]| > 5\sigma_{\overline{w}} \Rightarrow k_{FLR} = k. \tag{7}$$

The required delay for the current sample alignment is given by:

$$k_{sync} = k_{FLR} - k_{FL} + 1, \tag{8}$$

and the local wavelet coefficients are delayed by k_{sync} as follows:

$$\overline{w}^*_L[k] = \overline{w}_L[k - k_{sync}]. \tag{9}$$

Therefore, the local wavelet coefficients are aligned with the remote-sent ones using only the fault inception time detection information without the need for additional information such as system configuration, GPS, or communication channel latency.

H. DIFFERENTIAL WAVELET COEFFICIENTS (BLOCK 8)

Based on the traditional method based on phasor currents, the differential calculation is applied directly to the aligned wavelet coefficients $\overline{w}_{LR}$ and $\overline{w}^*_L$. The operating wavelet coefficient (w_{op}) and the restraint wavelet coefficient (w_{res}) are computed at each sampling time as follows:

$$w_{op}[k] = \left|\overline{w}^*_L[k] + \overline{w}_{LR}\right|, \tag{10}$$
$$w_{res}[k] = \left|\overline{w}^*_L[k]\right| + \left|\overline{w}_{LR}\right|. \tag{11}$$

I. DIFFERENTIAL ENERGY (BLOCK 9)

The energy of the first-decomposition level wavelet coefficients is given by:

$$\mathcal{E}_{op}[k] = \sum_{n=k-\Delta k+1}^{k} w^2_{op}[k], \tag{12}$$

$$\mathcal{E}_{res}[k] = \sum_{n=k-\Delta k+1}^{k} w^2_{res}[k], \tag{13}$$

where $k > \Delta k - 1$. Considering a phase-segregated transmission line differential protection, the proposed method uses the following energy pairs: $\{\mathcal{E}_{opA}, \mathcal{E}_{resA}\}$, $\{\mathcal{E}_{opB}, \mathcal{E}_{resB}\}$, and $\{\mathcal{E}_{opC}, \mathcal{E}_{resC}\}$.

J. TRIP LOGIC (BLOCK 10)

Similar to the traditional line differential protection (87L), the proposed wavelet-based unit (87LW) also uses differential quantities for fault detection. However, rather than low-frequency information from operating and restraint currents, the proposed method uses high-frequency information from operating and restraint wavelet coefficient energies, defined in (12) and (13). This work proposes three phase-segregated units taking into account the differential energy pairs $\{\mathcal{E}_{opA}, \mathcal{E}_{resA}\}$, $\{\mathcal{E}_{opB}, \mathcal{E}_{resB}\}$, and $\{\mathcal{E}_{opC}, \mathcal{E}_{resC}\}$.

Fig. 4 depicts the flowchart for the proposed fault detection logic (TRIP logic), which is able to discriminate between internal and external faults. The local differential protection operates independently on the remote differential protection, and the TRIP command can be issued by either of these two relays, as shown in Fig. 1.

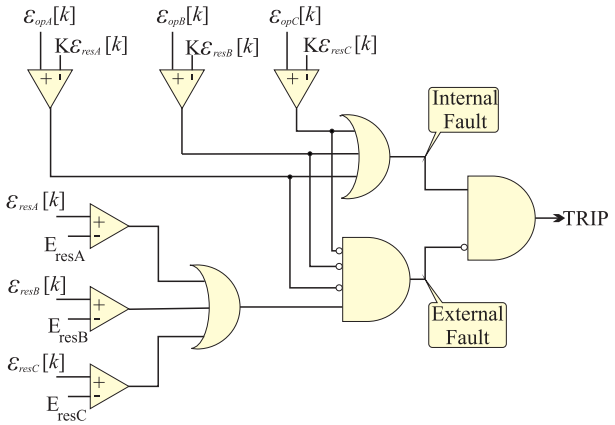

FIGURE 4. Flowchart: trip logic.

1) LINE ENERGIZATION

Energizing a transmission line provides the worst inrush conditions [32]. In order to evaluate the performance of the proposed method, an energization test was carried out by the local terminal, with the remote terminal remaining open. When an energization is detected, a subroutine is activated by modifying the slope to accommodate this phenomenon.

Fig. 5(a) shows the current measured at the local terminal, resulting from the local terminal energization, which is completely capacitive. In this condition, the remote current measurements are null; therefore, $\mathcal{E}_{res} \approx \mathcal{E}_{op}$. In Fig. 5(b), the energization detection occurs after the search window with N samples, which corresponds to the TW transit time of the wave plus the communication time between the terminals. As an example, where the TW transit time is estimated through the length of the TL and the TW velocity [23], equivalent to 10 samples, added to the maximum communication time of 5 ms or 80 samples, totaling a search window of 90 samples with a sampling frequency of 15.36 kHz. After energizing confirmation, a safety mode is activated, changing the protection scheme to the overcurrent function based on the wavelet energy from only the terminal energized.

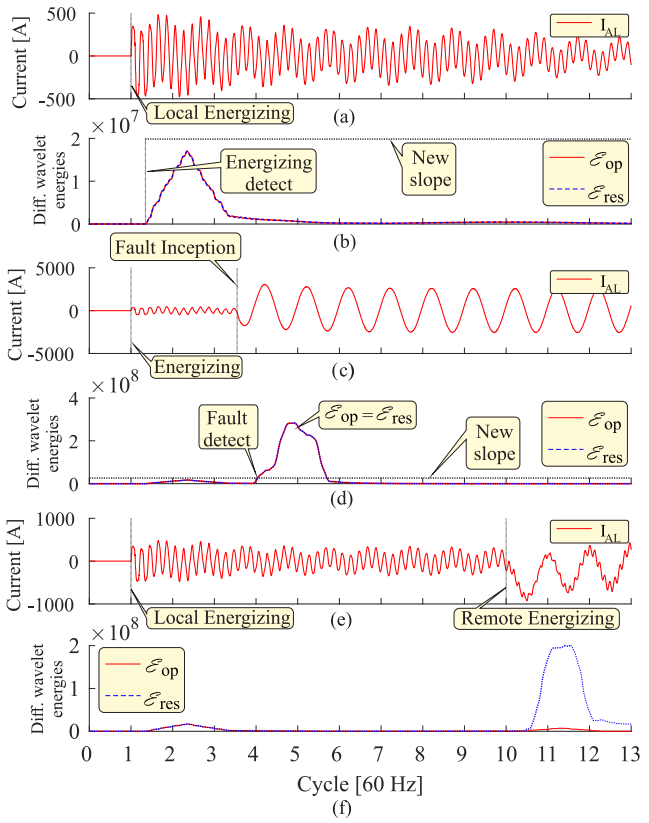

FIGURE 5. Local terminal energization (a) and (b); Local terminal energization followed by a single-phase-to-ground fault (c) and (d); Full TL energization, 1st local terminal close followed by remote terminal.

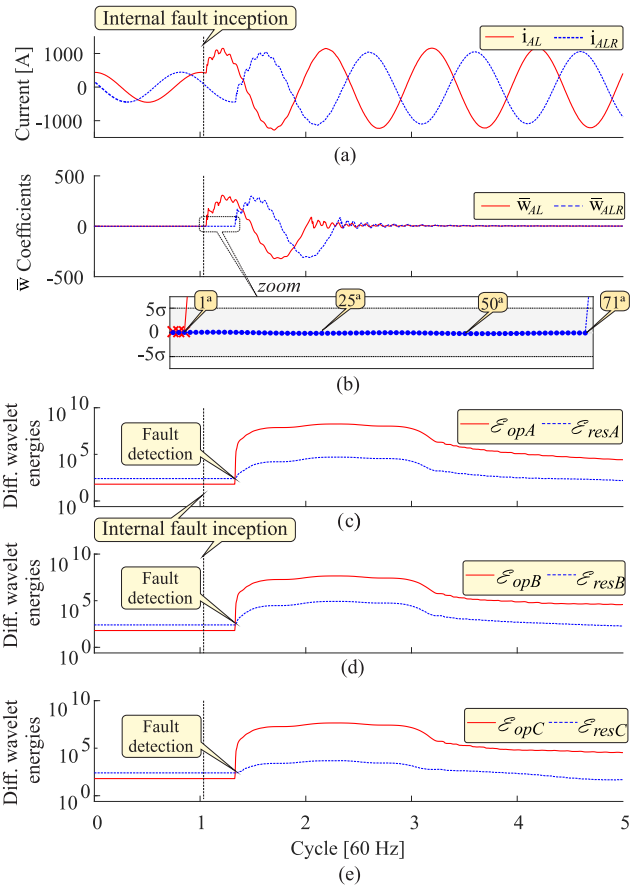

FIGURE 6. Internal fault in the protected TL: (a) Local current at the local terminal and remote current from the remote terminal; (b) Equivalent border wavelet coefficients; (c) Differential energies: Unit αA; (d) Differential energies: Unit αB; (e) Differential energies: Unit αC.

Therefore, a new threshold is defined based on a previous TL energization test. If this limit is exceeded, a TL fault is identified.

Fig. 5(c) shows the phase current after TL energizing followed by a single-phase-to-ground fault. According to Fig. 5(d), the fault causes an abrupt increase in the operating energy, rising above the new slope defined for the energizing condition, characterizing an internal fault. Figs. 5 (e) and (f) depict the case of a complete energization; both terminals are connected to the network, and at this moment, there is information from both terminals enabling the calculation of the restraint energy that rises abruptly, therefore acting safely during LT energization.

2) INTERNAL FAULT

When (5) is true, a disturbance is detected. Then, the differential protection units are triggered, and an internal fault is detected whenever at least one of the following conditions is fulfilled (Fig. 4):

$$\mathcal{E}_{opA}[k] > K\mathcal{E}_{resA}[k], \tag{14}$$

$$\mathcal{E}_{opB}[k] > K\mathcal{E}_{resB}[k], \tag{15}$$

$$\mathcal{E}_{opC}[k] > K\mathcal{E}_{resC}[k], \tag{16}$$

where K is the slope of the 87LW units.

As an example, Fig. 6 depicts the local and remote-sent current waveforms, their respective improved wavelet coefficients, and the differential energies in phases A, B, and C for an internal SLG fault involving phase A and ground, with a fault inception angle of 90° and considering the local terminal as a reference.

According to Fig. 6(b), $\overline{w}_{AL}$ and $\overline{w}_{ALR}$ present small values during pre-fault period, attending (5). After the fault initiation, $\overline{w}_{AL}$ and $\overline{w}_{ALR}$ extrapolate their respective thresholds. In this case, the alignment occurs for $ksync = 71$ in accordance with (8). Regarding the differential energies [Figs. 6(c)-(e)], $\mathcal{E}_{op} < K\mathcal{E}_{res}$ for all phase differential units during the pre-fault period. After the alignment, $\mathcal{E}_{op} > K\mathcal{E}_{res}$ in all phases, fulfilling the conditions expressed in (14) - (16), and a trip command is emitted.

3) EXTERNAL FAULT

A disturbance is detected as an external fault if (14) - (16) are not fulfilled and at least one of the following conditions is true:

$$\mathcal{E}_{resA}(k) > E_{resA}, \tag{17}$$

$$\mathcal{E}_{resB}(k) > E_{resB}, \tag{18}$$

$$\mathcal{E}_{resC}(k) > E_{resC}. \tag{19}$$

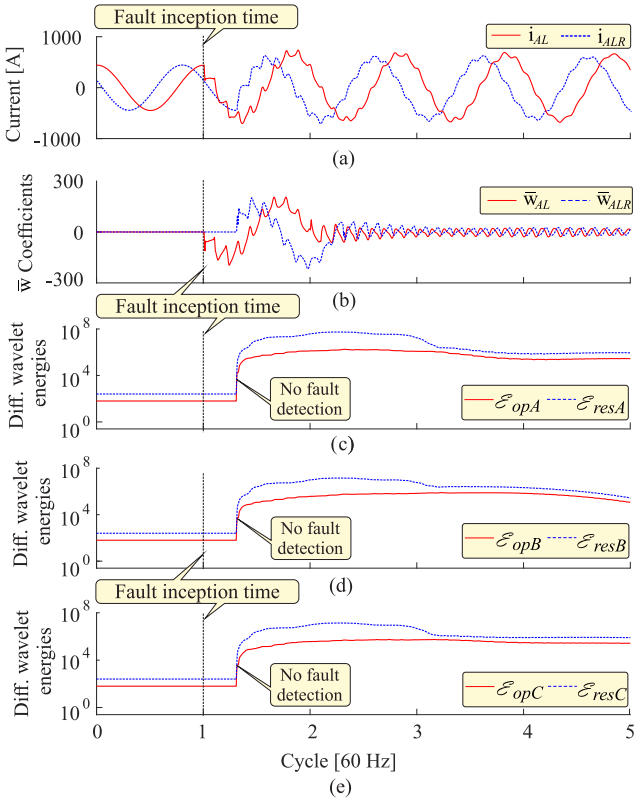

FIGURE 7. External fault: (a) Local current at the local terminal and remote current from the remote terminal; (b) Equivalent border wavelet coefficients; (c) Differential energies: Unit αA; (d) Differential energies: Unit αB; (e) Differential energies: Unit αC.

The energy threshold E_{res} is defined according to [33] as:

$$E_{res} = 3\mu_{\mathcal{E}} = \frac{3}{k_2 - k_1 + 1} \sum_{n=k_1}^{k_2} \mathcal{E}_{res}^{w}(n), \qquad (20)$$

where $\mu_{\mathcal{E}}$ is the computed average value from a dataset of $\mathcal{E}_{res}$, with k_1 and k_2 corresponding to arbitrary samples taken during the steady-state.

Fig. 7 depicts the local and remote-sent current waveforms, their respective improved wavelet coefficients, and the differential energies in phases A, B, and C for an SLG fault involving both phase A and ground, but external to the line protection zone. Unlike the internal fault, the restraint energies $\mathcal{E}_{res}$ tend to be larger than $\mathcal{E}_{op}$ [Figs. 7(c)-(e)], confirming the external fault detection.

III. PERFORMANCE ASSESSMENT

This section presents the assessment of the proposed wavelet-based transmission line differential protection (87LW) for events such as internal faults, external faults, and faults with CT saturation. Its performance was compared with a conventional transmission line percentage differential protection (87L). Fig. 8 depicts the 230 kV/60 Hz power system simulated on the Alternative Transients Program (ATP), with its transmission lines modeled through the JMarti frequency-dependent routine. The protected line of 200 km length presents four transposition points, following the scheme 1/6 + 1/3 + 1/3 + 1/6. The adjacent lines of 20 km length are connected in bars 2 and 3. The CTs are positioned in both protected line terminals according to [34].

The simulation time step was $1/f_{s1} = 6.5\ \mu$s, where $f_{s1} = 153.600$ kHz. After a filtering process through a third-order Butterworth anti-aliasing low-pass filter with a cutoff frequency of $f_s/2$ Hz, the signals were downsampled at f_s. The proposed method uses a sampling rate (f_s) of 15.36 kHz. Then, the discrete-time signals have 256 samples per cycle of 60 Hz, which allows the proper extraction of fault-induced transients [28]. Conversely, the adopted conventional protection 87L uses a sampling frequency of 960 Hz (i.e., 16 samples per cycle of 60 Hz), a capacitive current compensation technique [35], and the modified cosine filter for phasor estimation [36].

Tables 1 and 2 describe all fault parameters changed for the massive simulation of external and internal faults, respectively. All simulated cases were obtained by changing only one parameter at a time, while the others were set as their default values, namely: fault inception angle of $\theta_f = 0°$ (referenced to the phase A voltage), phase-to-ground fault resistance $R_g = 0\ \Omega$, phase-to-phase fault resistance $R_f = 0\ \Omega$, and fault location at $d_f = 100$ km, i.e, on the middle of the protected line.

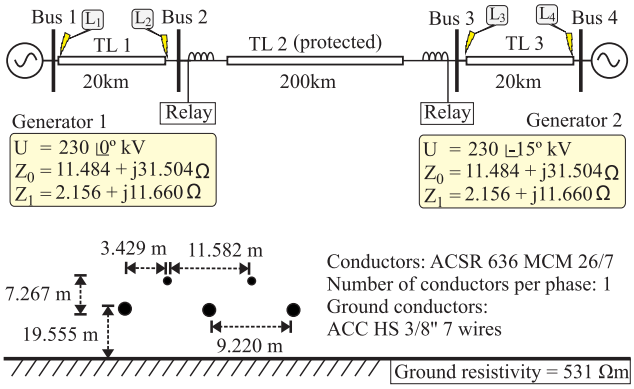

FIGURE 8. Power electric system.

TABLE 1. Fault parameters used in external faults.

Fault type	AG, BG, CG, AB, BC, CA, ABG, BCG, ACG, ABC
R_g R_f	0, 100, 200, ..., 800, 900, 1000 [Ω]
Fault location	L_1, L_2, L_3, L_4
θ_f	0°, 15°, 30°,...,150°, 165°, 180°
Total cases	5720

A. INTERNAL FAULT

The wavelet coefficients present random values during the steady state due to measured signal noise. Then, operating

TABLE 2. Fault parameters used in internal faults.

Fault type	AG, BG, CG, AB, BC, CA, ABG, BCG, ACG, ABC
R_g R_f	0, 100, ..., 900, 1000 [Ω]
Fault location	0, 20, 40, ..., 160, 180, 200 [km]
θ_f	0°, 15°, 30°,...,150°, 165°, 180°
Total cases	15730

and restraint energies usually present a relatively flat magnitude as a noise function. After the fault inception time and the signal alignment, the operating and restraint energies present hard changes such that the operating point goes to the operating or restraint regions in case of internal faults or external faults, respectively.

Fig. 9 depicts the trajectories of the operating points in a differential characteristic plane for some selected AG (phase-A-to-ground) internal and external faults. The restraint and operating energies, per sampling time, form the ordered pair ($\mathcal{E}^w_{res}$,$\mathcal{E}^w_{op}$). The selected faults present extreme inception angles for AG faults, equal to 0° and 90°, to highlight the influence of this fault parameter. AG internal faults with $\theta_f \approx 0°$ present damped or no transients. Consequently, the operating point moves to the operating region more slowly, causing delays in the fault detection. Conversely, the operating points quickly converge in the operating zone when relevant transients exist in the fault, such as in AG internal faults with $\theta_f \approx 90°$. For instance, the AG internal fault with $\theta_f = 90°$ was detected in the 1^{st} sample after the current alignment, whereas the AG internal fault with $\theta_f = 0°$ was detected only in the 5^{th} sample [Fig. 9], which is still k^{st}.

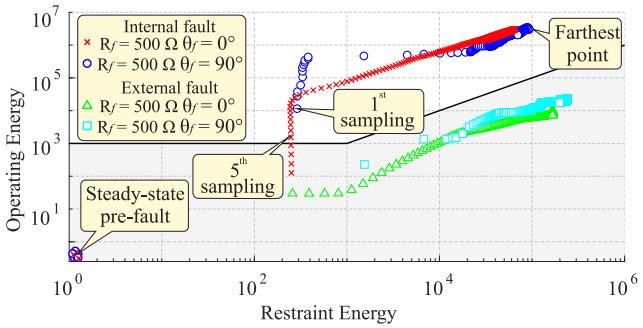

FIGURE 9. Characteristic trajectories for internal faults and external faults in the percentage plane.

The proposed method was extensively evaluated by applying several internal faults, including, besides the cases described in Table 2, faults with outfeed conditions. Fig. 10 depicts the operating points for some cases of internal faults with variations in both fault resistance and fault location according to Table 2, all of them presenting a fault inception angle of 90°, in order to verify the influence of fault resistance and fault location on the performance of the proposed method. For each case, only the most representative operating point taken during the fault regime is plotted in Fig 10, i.e., the highest $\mathcal{E}^w_{op}$.

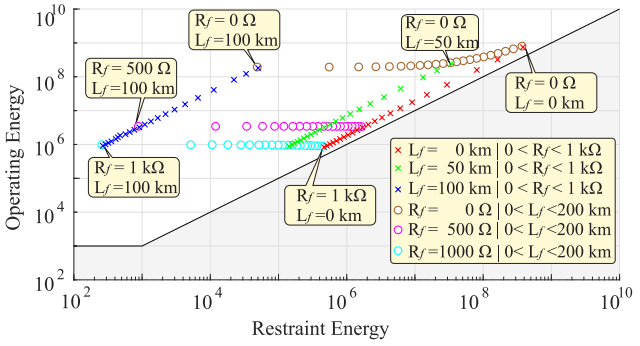

FIGURE 10. Mapping of the percentage wavelet plan: mass simulation AG fault with fault inception angle 90°.

The point located in the operating region indicates the proposed protection detected the fault and issued the trip successfully. Therefore, it is possible to map the effects on the operating of the wavelet differential protection according to the variation of the parameters described in Table 1.

The fault location (circular points) causes a reduction in the restraint energy as it approaches to the line center. When the fault takes place at the line center, $\overline{w}$ extrapolates the thresholds in (5) in currents from both line terminals, at the same time, with equal polarities. Based on (10) and (11), $\mathcal{E}_{res}$ and $\mathcal{E}_{op}$ will result in minimum and maximum values, respectively. When the fault takes place near the line terminals, the delay between the coefficients $\overline{w}_L$ and $\overline{w}_{LR}$ increases, resulting in an increase in the energy $\mathcal{E}_{res}$. However, in the evaluated cases, the fault location parameter did not compromise the protection operation, since all faults resulted in points in the operation zone.

When the fault resistance increases, it leads to a reduction in both energies ($\mathcal{E}_{op}$ and $\mathcal{E}_{res}$) because the transient amplitude is reduced. This results in an inclined path profile in the wavelet differential plane (x points in Fig. 10).

B. EXTERNAL FAULTS

The performance of the proposed method was also assessed for external faults according to Table 1. Fig. 11 shows the most representative operating point for each assessed external fault. According to Fig. 11, all operating points remained in the restraint region. Therefore, the proposed method was correctly operated for all external faults, and no trip was issued.

C. EXTERNAL FAULTS WITH CT SATURATION

The current measurement is inaccurate when a CT saturates, resulting in differential currents larger than the reference value. Therefore, differential protection might misoperate whenever CT saturates during external faults [37].

To analyze this phenomenon, fault simulations with variations in fault type, fault resistance, and CT saturation

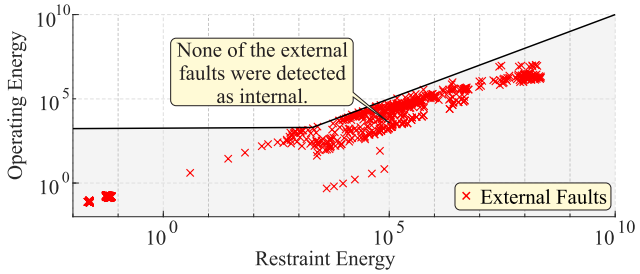

FIGURE 11. Percentage wavelet plan with maximum points of external faults.

severity were performed according to the database generated considering the variable shown in Table 3.

TABLE 3. External fault with TC saturation parameters.

Fault type	AG, AB, ABG, ABC
R_g R_f	0, 5, 10 [Ω]
% Saturation	10, 15, 25

According to the criteria demonstrated in section II-J, the detection of an external fault occurs even before the CT saturation, enabling the protection secure mode that extends the TRIP confirmation window to half a cycle to accommodate the differential energy accumulated in the saturation period. That is, for a disturbance to be confirmed as an internal fault, the condition $\mathcal{E}^w_{op} > \mathcal{E}^w_{res}$ must be confirmed by at least 1/2 cycle. In this way, it is possible to accommodate the differential energy accumulated due to the CT saturation period, preventing misoperation during an external fault with CT saturation.

Fig. 12 (a) depicts the phase A local current for a case of an external fault of type AG with $R_g = 0\ \Omega$, presenting a CT saturation of about 25%. Fig. 12 (b) shows the improved wavelet coefficients, which present abrupt variations when saturation occurs, resulting in imprecise differential energies, as shown in Fig. 12 (c), increasing the operating energy and reducing the restraint energy. Therefore, fulfill at least one of the conditions (13)-(15) for less than 1/2 cycle. This methodology did not detect external faults with CT saturation as internal faults, ensuring relay security.

D. COMPARISON BETWEEN 87L AND 87LW UNITS

As aforementioned, the traditional percentage differential protection unit 87L uses current phasors, requires voltage measurements to remove capacitive charging current, and performs synchronization via GPS [4]. Conversely, the proposed 87LW unit uses differential wavelet coefficient energy instead of phasor estimation, does not use the capacitive current compensation technique, and performs data alignment based on the traveling wave theory with no need for GPS synchronization.

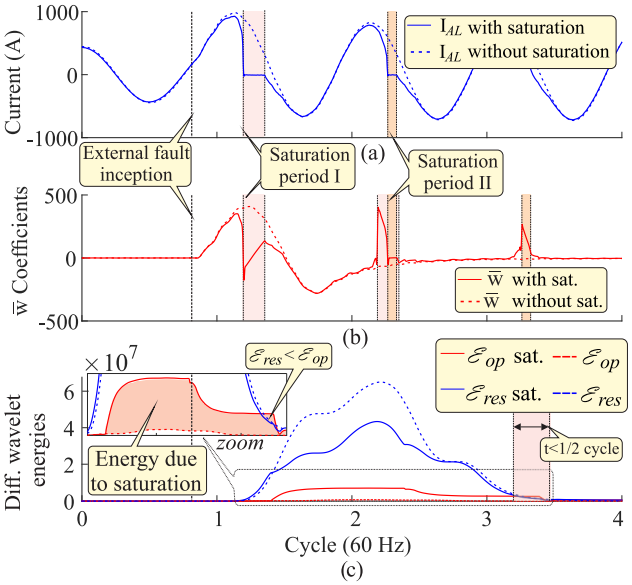

FIGURE 12. Effect of CT saturation. (a) Phase A current. (b) Equivalent wavelet coefficient. (c) Operating and restraint energies.

TABLE 4. Fault detection rate.

Fault types	% Diff. protection (Fourier)		Wavelet % Diff. Protection	
	87L (%)	87L(ms)	87LW(%)	87LW(ms)
AG	96	31.4±7.6	100	6.6±0.51
BG	95.8	30.7±6.9	100	6.5±0.42
CG	96.3	31.1±7.2	100	6.6±0.55
ABG	100	25±4.5	100	6.3±0.45
BCG	100	25.2±4.2	100	6.4±0.44
ACG	100	24.7±4.2	100	6.3±0.48
AB	100	25.5±4.8	100	6.4±0.42
BC	100	25.1±4.3	100	6.3±0.4
CA	100	25.2±4.3	100	6.5±0.46
ABC	100	24.7±4.9	100	6.4±0.37

Table 4 presents the success rates (%) of the proposed 87LW and existing 87L percentage differential protection methods considering the cases summarized in Table 2. The traditional differential method did not ensure the proper operation in the entire range of the fault impedance because faults with outfeed conditions and high impedances were not detected. On the other hand, the proposed method presented a success rate of 100%, overcoming the existing limitations of the conventional method.

The fault detection time is a fundamental criterion in protection because faults generate mechanical stresses to equipment, reducing their life cycle. To increase the reliability in fault detection, the proposed 87LW unit adopted the criterion of consecutive confirmation samples. Then, a fault is confirmed if the detection criterion (16)-(18) is satisfied by ten consecutive samples. Due to the phasor

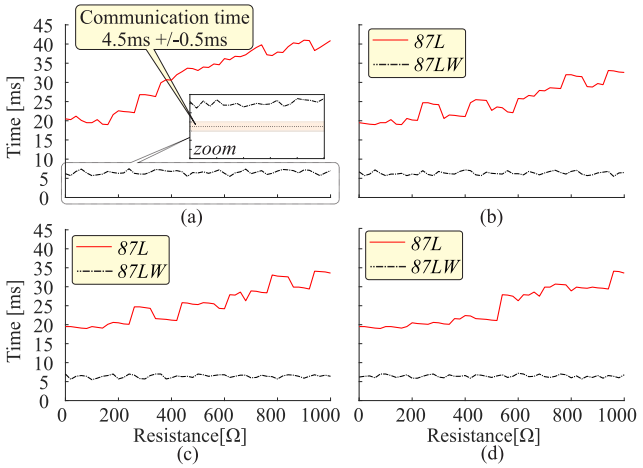

FIGURE 13. Effect of the fault impedance variation on the detection time for faults: (a) Single-phase: AG; (b) Double-phase-ground: ABG; (c) Double-phase: AB;(d) Three-phase: ABC.

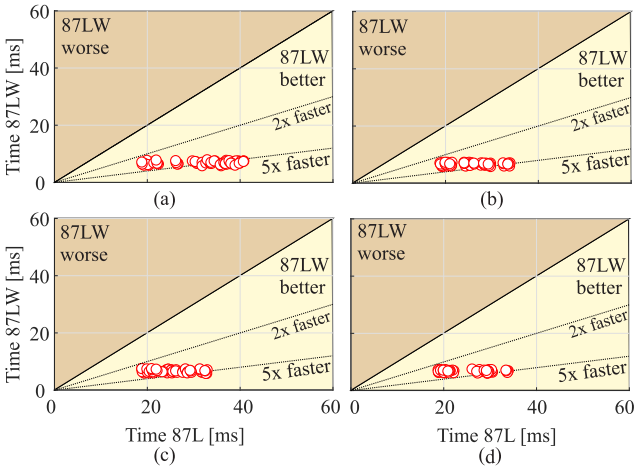

FIGURE 14. Effect of the fault resistance variation on the detection time for faults: (a) single-phase; (b) Double-phase; (c) Double-phase-ground; (d) Three-phase.

estimation, the conventional method requires a longer time, which is around one cycle, for adequate phasor convergence.

Fig. 13 depicts the delay time in fault detection of both 87L and 87LW units for variations in the fault resistance, for AG, ABG, AB, and ABC fault types.

According to Fig. 13, the operation time of the 87LW unit was scarcely affected by the fault resistance variation, presenting an average detection time of 6.6 ms with a standard deviation of 0.51 ms. Conversely, the traditional 87L unit presented larger delays as the fault resistance increased, leading to an average detection time of 31.4 ms with a standard deviation of 7.6 ms. Emphasizing that the complete process of data acquisition, communication between terminals, and signal reception accounts for an average of 4.5 ms of the total detection time. In other words, the proposed algorithm is able to identify any fault situation with an average time of 2 ms after receiving the information from the remote terminal, being, therefore, in some cases, almost 10 times faster than the conventional method.

Fig. 14 shows scatter plots that compare both 87L and 87LW units regarding their operation speeds for cases addressed in Fig. 13. Each point on the graph represents one fault scenario, and the straight shows the speed relationship between the 87L and 87LW units. According to Fig. 14, when both methods are compared case by case, the 87LW unit always detects faults faster than the conventional unit. For instance, the proposed 87LW is about 5 times faster than the 87L in detecting high resistance fault cases, disregarding the cases detected by the 87LW and not detected by the 87L unit.

E. A SPECIAL CASE: INTERNAL FAULT WITH OUTFEED

A single-phase-to-ground internal fault in phase A (AG fault) was simulated at TL2, 5 km away from Bus 3, with fault impedance of $R_f = 700\ \Omega$. The performance analysis of the conventional 87L and the proposed 87LW functions is represented in Fig. 15. Fig. 15 (a) shows the magnitudes of the local phase A (i_{AL}) and the remote-sent phase A (i_{ALR}) currents. After the fault takes place, there is an increase in the local phase A current and a slight reduction in the remote-sent phase A current, such that it remains in the same direction from pre-fault period. It happens because the load current is much larger than the fault current contribution coming from the remote terminal.

After the signal alignment, the operating current (I_{opA}) of the conventional differential phase A unit (87LA) remains below $SLP.I_{resA}$. Consequently, the fault is not detected [Fig. 15 (b)]. Nevertheless, the conventional differential negative sequence unit (87LQ) provides the necessary security for fault detection [Fig. 15 (c)], but usually a delay in the operation of the sequence units is used to prevent false detection during the transitory period. In other words, the trip command is only issued if the operating conditions is fulfilled ceaselessly during one cycle after fault detection [38]. In this case, since 87LQ units detected the fault after 36.7 ms (2.2 cycles), the trip command is issued only in 53.4 ms (3.2 cycles).

Fig. 15 (d) shows that the proposed 87LWA unit issued the trip in 5.1 ms (0.3 cycles) because $\mathcal{E}_{opA}$ becomes larger than $SLP.\mathcal{E}_{resA}$ just after the signal alignment procedure. As a result, the proposed method is robust and fast to faults during outfeed conditions.

F. COMPARISON WITH EXISTING METHODS

In Table 5, a general performance comparison is shown between conventional differential techniques (87L), traveling wave line current differential element (87TW), and the proposed method (87LW). The presence of a communication channel between the terminals is inherent to all methods, and they are capable of operating under Current Transformer (CT) saturation conditions. However, for faults occurring during transmission line energization, the 87L protection fails to detect the fault, as well as in situations of outfeed

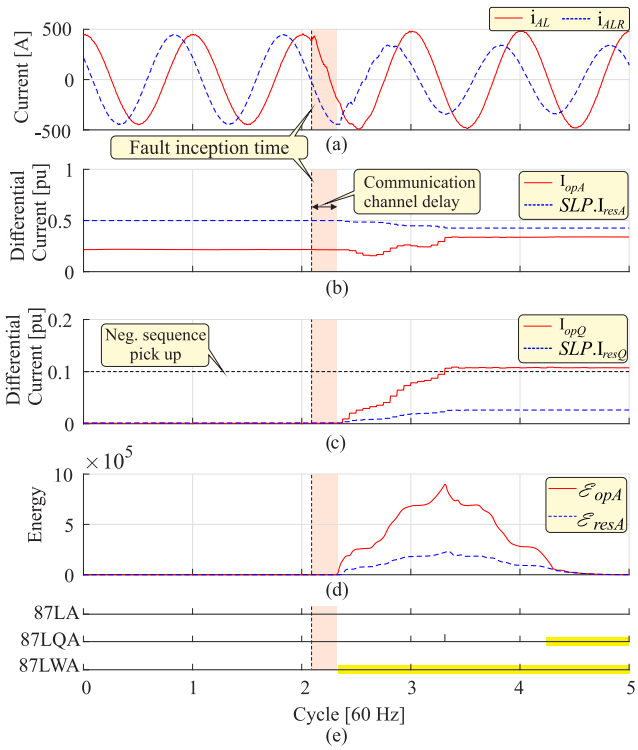

FIGURE 15. Internal fault with outfeed: (a) Phase A local and remote-sent currents; (b) Differential currents of conventional 87LA unit; (c) Differential currents of conventional 87LQ unit; (d) Differential energies: Unit αA; (e) Trip command issue.

faults. Methods based on traveling waves (TW) [39] are highly dependent on the identification of wave arrival times. In situations with significant noise, or during faults with certain fault inception angles that do not generate transients in the network, detecting the arrival of these wavefronts is not possible.

The proposed method (87LW) ensures safe and reliable operation across all presented fault scenarios, since it is based on the operating and restraint energies of high-frequency components obtained with advanced wavelet processing, which in turn are able to detect and confirm the fault for several cycles after the event onset. Conversely, this is not seen in traveling wave-based protections, which are highly dependent on identifying the first wavefront of the faulted signals.

G. COMPUTATIONAL BURDEN AND IMPLEMENTATION FEASIBILITY IN A MODERN DIGITAL SIGNAL PROCESSOR (DSP)

The exchange of information between terminals is already common practice today. The proposed transmission line differential protection was designed with a sampling rate of 15360 Hz, which is in accordance with the current technology used in protective relays. The wavelet filter chosen was the db(4). Therefore, the protection performs all floating-point operations in a time less or equal to one sampling time ($\frac{1}{15360} \approx 65\ \mu s$). Additionally, a data window of 256 samples per 60 Hz cycle is generated, whose length

TABLE 5. Comparison between conventional differential protection methods (87L), traveling wave differential protection (87TW), and wavelet differential protection (87LW).

	87L	87LW	87TW
Communication	✓	✓	✓
Saturation	✓	✓	✓
Energization		✓	✓
Outfeed		✓	✓
Without transients	✓	✓	
High speed		✓	✓

is much smaller than the one used by traveling wave-based protections, which usually use sampling rates close to 1 MHz. The computational load required for the proposed method can be calculated by accounting for the number of floating-point operations (FLOPs), which calculates the amount of addition and multiplication operations.

The proposed method is based solely on addition and multiplication operations. For the calculate signal processing steps and Clarke transform, 168 FLOPs were required. In the case of using the db(4) mother wavelet, a coefficient of energy limited wavelet requires only 38 FLOPs per sampling time, which is slightly higher than that described in [28], due to the addition of the implementation of the equivalent coefficient that improves the algorithm's sensitivity. For the synchronization steps, differential calculation, and trip decision, 415 FLOPs are necessary, totaling 621 FLOPs. To implement synchronization between local and remote terminal signals, memory management needs to be considered to store one-third of a cycle for each phase alpha component. Considering a 32-bit architecture commonly used in computer systems, meaning each number is represented by 32 bits in the system memory, only a memory space of 1 KByte operating in the format of a circular buffer will be required.

As a benchmark, the TMS320xF2833x floating-point DSP for real-time operation analysis in [40], the proposed method would require about 31.05μs per sampling time to perform wavelet differential protection processing, a time lower than the available 65μs. Therefore, the proposed method could be correctly implemented on current equipment.

IV. CONCLUSION

This paper presents a transmission line differential protection based on the boundary discrete wavelet transform with wavelet signals aligned based on traveling wave concepts without the need for external synchronization elements. The performance of the proposed method was evaluated with massive simulations of internal faults, including outfeed conditions, high impedance faults, CT saturation, TL energization, external faults, and a self-alignment scheme.

Unlike the conventional differential protection (87L), the proposed method (87LW) did not present significant variations in the fault detection time with the increase of the impedance, leading to the fastest response in the fault

detection for the entire operating range. It presented a success rate of 100 % for internal faults and provided safe operation for external faults. Additionally, it does not require the suppression of the capacitive current, so there is no need for voltage measurements.

The proposed method is promising for transmission line protection since it was designed for real-time applications with an implementation that uses a small computational burden, combines the speed of traveling waves for the alignment of signals without the need for external agents, and it has well-defined restraint and operating characteristics variables providing a safety trip decision in adverse conditions for the entire transmission line length.

ACKNOWLEDGMENT

The author would like to acknowledge Santa Cruz State University.

REFERENCES

[1] I. Nikoofekr and J. Sadeh, "Nature of fault determination on transmission lines for single phase autoreclosing applications," *IET Gener., Transmiss. Distrib.*, vol. 12, no. 4, pp. 903–911, Feb. 2018.

[2] E. O. Schweitzer, B. Kasztenny, A. Guzmán, V. Skendzic, and M. V. Mynam, "Speed of line protection—Can we break free of phasor limitations?" in *Proc. 68th Annu. Conf. Protective Relay Engineers*, Mar. 2015, pp. 448–461.

[3] M. J. Thompson, "Percentage restrained differential, percentage of what?" in *Proc. 64th Annu. Conf. Protective Relay Engineers*, 2011, pp. 278–289.

[4] G. Ziegler, *Numerical Differential Protection: Principles and Applications*. Hoboken, NJ, USA: Wiley, 2012.

[5] *IEEE Guide for Application of Digital Line Current Differential Relays Using Digital Communication*, IEEE Standard C37.243-2015, 2015, pp. 1–72.

[6] S. Dambhare, S. A. Soman, and M. C. Chandorkar, "Adaptive current differential protection schemes for transmission-line protection," *IEEE Trans. Power Del.*, vol. 24, no. 4, pp. 1832–1841, Oct. 2009.

[7] S. Miao, P. Liu, and X. Lin, "An adaptive operating characteristic to improve the operation stability of percentage differential protection," *IEEE Trans. Power Del.*, vol. 25, no. 3, pp. 1410–1417, Jul. 2010.

[8] K. Solak, W. Rebizant, and A. Klimek, "Fuzzy adaptive transmission-line differential relay immune to CT saturation," *IEEE Trans. Power Del.*, vol. 27, no. 2, pp. 766–772, Apr. 2012.

[9] *IEEE Guide for Synchronization, Calibration, Testing, and Installation of Phasor Measurement Units (PMUS) for Power System Protection and Control*, IEEE Standard C37.242-2021 (Revision IEEE Std C37.242-2013), 2021, pp. 1–98.

[10] K. Fodero, C. Huntley, D. Whitehead, and B. Kasztenny, "A novel scheme for wide-area time synchronization," in *Proc. 10th IET Int. Conf. Develop. Power Syst. Protection (DPSP)*, 2010, pp. 1–5.

[11] N. Villamagna and P. A. Crossley, "A symmetrical component-based GPS signal failure-detection algorithm for use in feeder current differential protection," *IEEE Trans. Power Del.*, vol. 23, no. 4, pp. 1821–1828, Oct. 2008.

[12] G. Benmouyal, "The trajectories of line current differential faults in the alpha plane," in *Proc. 32nd Annu. Western Protective Relay Conf.*, 2005, p. 19.

[13] G. Benmouyal and J. B. Mooney, "Advanced sequence elements for line current differential protection," in *Proc. 33rd Annu. Western Protective Relay Conf.*, 2005, p. 19.

[14] B. Kasztenny, G. Benmouyal, H. J. Altuve, and N. Fischer, "Tutorial on operating characteristics of microprocessor-based multiterminal line current differential relays," in *Proc. 38th Annu. Western Protective Relay Conf.*, 2011, pp. 1–30.

[15] E. O. Schweitzer and D. Hou, "Filtering for protective relays," in *Proc. IEEE WESCANEX Commun., Comput. Power Modern Environ.*, May 1993, pp. 15–23.

[16] F. Wilches-Bernal, A. Bidram, M. J. Reno, J. Hernandez-Alvidrez, P. Barba, B. Reimer, R. Montoya, C. Carr, and O. Lavrova, "A survey of traveling wave protection schemes in electric power systems," *IEEE Access*, vol. 9, pp. 72949–72969, 2021.

[17] B. Bhalja and R. P. Maheshwari, "Wavelet transform based differential protection scheme for tapped transmission line," in *Proc. IEEE Int. Conf. Ind. Technol.*, vol. 14, Dec. 2006, pp. 1004–1008.

[18] N. Pahade, P. S. Patii, and A. Badar, "Wavelet based transmission line differential protection scheme," in *Proc. Int. Conf. Power Embedded Drive Control (ICPEDC)*, Mar. 2017, pp. 522–526.

[19] F. B. Costa, "Fault-induced transient detection based on real-time analysis of the wavelet coefficient energy," *IEEE Trans. Power Del.*, vol. 29, no. 1, pp. 140–153, Feb. 2014.

[20] F. B. Costa, "Boundary wavelet coefficients for real-time detection of transients induced by faults and power-quality disturbances," *IEEE Trans. Power Del.*, vol. 29, no. 6, pp. 2674–2687, Dec. 2014.

[21] M. Wen, D. Chen, and X. Yin, "Instantaneous value and equal transfer processes-based current differential protection for long transmission lines," *IEEE Trans. Power Del.*, vol. 27, no. 1, pp. 289–299, Jan. 2012.

[22] L. Tang, X. Dong, S. Luo, S. Shi, and B. Wang, "A new differential protection of transmission line based on equivalent travelling wave," *IEEE Trans. Power Del.*, vol. 32, no. 3, pp. 1359–1369, Jun. 2017.

[23] F. B. Costa, A. Monti, F. V. Lopes, K. M. Silva, P. Jamborsalamati, and A. Sadu, "Two-terminal traveling-wave-based transmission-line protection," *IEEE Trans. Power Del.*, vol. 32, no. 3, pp. 1382–1393, Jun. 2017.

[24] K. M. Silva, A. M. P. Escudero, F. V. Lopes, and F. B. Costa, "A wavelet-based busbar differential protection," *IEEE Trans. Power Del.*, vol. 33, no. 3, pp. 1194–1203, Jun. 2018.

[25] R. P. Medeiros and F. B. Costa, "A wavelet-based transformer differential protection: Internal fault detection during inrush conditions," *IEEE Trans. Power Del.*, vol. 33, no. 6, pp. 2965–2977, Dec. 2018.

[26] F. B. Costa, B. A. Souza, N. S. D. Brito, J. A. C. B. Silva, and W. C. Santos, "Real-time detection of transients induced by high-impedance faults based on the boundary wavelet transform," *IEEE Trans. Ind. Appl.*, vol. 51, no. 6, pp. 5312–5323, Nov. 2015.

[27] C. C. B. Oliveira, H. P. Schmidt, N. Kagan, and E. J. Robba, *Introdução a Sistemas Elétricos de Potência: Componentes Simétricas*. São Paulo, Brazil: Blucher, 2000.

[28] F. B. Costa and J. Driesen, "Assessment of voltage sag indices based on scaling and wavelet coefficient energy analysis," *IEEE Trans. Power Del.*, vol. 28, no. 1, pp. 336–346, Jan. 2013.

[29] I. Bárány and V. Vu, "Central limit theorems for Gaussian polytopes," *Ann. Probab.*, vol. 35, no. 4, pp. 1593–1621, Jul. 2007, doi: 10.1214/009117906000000791.

[30] H. Y. Li, E. P. Southern, P. A. Crossley, S. Potts, S. D. A. Pickering, B. R. J. Caunce, and G. C. Weller, "A new type of differential feeder protection relay using the global positioning system for data synchronization," *IEEE Trans. Power Del.*, vol. 12, no. 3, pp. 1090–1099, Jul. 1997.

[31] F. V. Lopes, K. M. Silva, F. B. Costa, W. L. A. Neves, and D. Fernandes, "Real-time traveling-wave-based fault location using two-terminal unsynchronized data," *IEEE Trans. Power Del.*, vol. 30, no. 3, pp. 1067–1076, Jun. 2015.

[32] H. A. Darwish, A.-M.-I. Taalab, and E. S. Ahmed, "Investigation of power differential concept for line protection," *IEEE Trans. Power Del.*, vol. 20, no. 2, pp. 617–624, Apr. 2005.

[33] R. P. Medeiros, F. B. Costa, and K. M. Silva, "Power transformer differential protection using the boundary discrete wavelet transform," *IEEE Trans. Power Del.*, vol. 31, no. 5, pp. 2083–2095, Oct. 2016.

[34] IEEE-PSRC. (2004). *EMTP Reference Models for Transmission Line Relay Testing*. [Online]. Available: https://www.pes-psrc.org/kb/report/074.pdf

[35] H. Miller, J. Burger, N. Fischer, and B. Kasztenny, "Modern line current differential protection solutions," in *Proc. 63rd Annu. Conf. Protective Relay Engineers*, Mar. 2010, pp. 1–25.

[36] D. G. Hart, D. Novosel, and R. A. Smith, *Modified Cosine Filters*. Raleigh, NC, USA: ABB Power T&D Company, 2000.

[37] *IEEE Guide for the Application of Current Transformers Used for Protective Relaying Purposes-Redline*, IEEE Standard C37.110, Apr. 2007.

[38] B. Kasztenny, N. Fischer, and H. J. Altuve, "Negative-sequence differential protection–principles, sensitivity, and security," in *Proc. 68th Annu. Conf. Protective Relay Engineers*, Mar. 2015, pp. 364–378.

[39] E. O. Schweitzer, B. Kasztenny, and M. V. Mynam, "Performance of time-domain line protection elements on real-world faults," in *Proc. 69th Annu. Conf. Protective Relay Engineers (CPRE)*, Apr. 2016, pp. 1–17.

[40] T. Instruments. *Technical Reference Manual Tms320x2833x, Tms320x2823x*. Accessed: Apr. 22, 2024. [Online]. Available: https://www.ti.com/lit/ug/sprui07/sprui07.pdf?ts=1714897858062

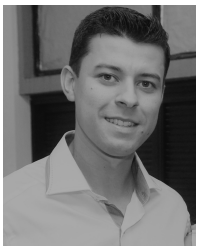

IGOR F. PRADO (Member, IEEE) received the B.Sc. degree in electrical engineering from the Federal Institute of Science and Technology of Bahia (IFBA), Brazil, in 2011, and the M.Sc. degree in methods for optimizing electrical power systems from the Federal University of ABC, Brazil, in 2013. He is currently pursuing the Ph.D. degree in electrical engineering with the Federal University of Rio Grande do Norte (UFRN), Brazil. He has experience in genetic algorithms applied to the optimization of electrical systems and has developed studies in the protection of transmission lines in the time domain. He has been an Assistant Professor with the Department of Engineering and Computing, Santa Cruz State University (UESC), since August 2014.

FLAVIO B. COSTA (Member, IEEE) received the B.Sc., M.Sc., and Ph.D. degrees in electrical engineering from the Federal University of Campina Grande (UFCG), Brazil, in 2005, 2006, and 2010, respectively. He was a Professor with the Federal University of Rio Grande do Norte (UFRN), Brazil, from 2010 to 2021. From 2010 to 2011 (one year), he was a Postdoctoral Fellow with UFCG. From December 2011 to March 2012 (three months), he was a Visiting Fellow with KU Leuven, Belgium. From June 2014 to July 2014 (two months), he was a Visiting Fellow with INESC Porto, Portugal. From August 2014 to September 2015 (11 months), he was a Postdoctoral Fellow with the Institute for Automation of Complex Power Systems (ACS), Rheinisch-Westflische Technische Hochschule Aachen (RWTH Aachen) University (one year), Germany. From November 2018 to October 2019 (one year), he was a Visiting Professor with TU Berlin, Germany. He has been an Assistant Professor with the Electrical and Computer Engineering Department, Michigan Technological University, since December 2021. His research interests include generation, transmission, and distribution systems, including power system protection, real-time analysis of power quality disturbances and faults, renewable energy systems, and smart-grid solutions.

KLEBER M. SILVA (Senior Member, IEEE) received the B.Sc., M.Sc., and Ph.D. degrees in electrical engineering from the University of Campina Grande, Brazil, in 2004, 2005, and 2009, respectively. Since 2009, he has been a Professor with the University of Brasilia, Brazil, and the Head of the Power System Protection Group. His research interests focus on power system protection, fault location, and electromagnetic transients. He is a member of SC B5-Protection and Automation Committee of CIGRE Brazil. He is an Senior Editor for the IEEE TRANSACTIONS ON POWER DELIVERY.

RODRIGO P. MEDEIROS (Member, IEEE) received the B.Sc., M.Sc., and Ph.D. degrees in electrical engineering from the Federal University of Rio Grande do Norte (UFRN), Natal, Brazil, in 2012, 2014, and 2018, respectively. From 2019 to 2020, he was a Postdoctoral Researcher with UFRN. He is currently an Associate Professor with UFRN. His research interests include power system protection, electrical machine drives, power grid parameter estimation, and digital signal processing.

BRUCE A. MORK (Senior Member, IEEE) received the B.S.M.E., B.S.E.E., and Ph.D. degrees in electrical engineering from North Dakota State University, in 1979, 1981, and 1992, respectively. From 1982 to 1986, he was a Design Engineer with Burns and McDonnell Engineering, Kansas City, MO, USA, in the areas of substation design, protective relaying, and communications. He joined as a Faculty Member with Michigan Technological University, Houghton, in 1992, where he is currently a Professor.